# Semi-active optimization control of space grid model with self-reset piezoelectric friction damper

**Yang Liu[1,2,*], Meng Zhan[3], Guangyuan Weng[4], Sheliang Wang[1]**

*1. College of Civil Engineering,
Xi'an University of Architecture and Technology, Xi'an 710055, China*

*2. School of Civil Engineering & Geodesy,
Shaanxi College of Communication Technology, Xi'an 710018, China*

*3. College of Architecture Engineering,
HuangHuai University, Zhumadian 463000, China*

*4. Mechanical Engineering College
Xi'an Shiyou University, Xi'an 710065, China*

*yangliu1106@163.com*

*ABSTRACT. This paper attempts to reduce the seismic hazards of building structure with an intelligent material called piezoelectric ceramics (PC). Specifically, the author designed a self-reset piezoelectric friction damper (SRPFD) based on laminated PC, and the number and position of dampers were optimized with genetic algorithm (GA) on the Matlab. On this basis, a large 24m×24m square pyramid space truss structure model was created, and the GA was optimized by the Gads toolbox. Then, 60 SRPFDs were selected to analyze the seismic response of the building structure. The results show that the control effect of the SRPFDs was improved by nearly 32.5% after the optimization. This research findings shed new light on semi-active optimization control of space grid models.*

*RÉSUMÉ. Cet article tente de réduire les risques sismiques de la structure d'un bâtiment avec un matériau intelligent appelé céramique piézoélectrique (PC). En particulier, l'auteur a conçu un amortisseur de friction piézoélectrique à réinitialisation automatique (SRPFD) à base de PC stratifié, et le nombre et la position des amortisseurs ont été optimisés avec un algorithme génétique (GA) sur Matlab. Sur cette base, un grand modèle de structure en treillis spatiaux pyramidaux carrés de 24 m × 24 m a été créé et l'AG a été optimisée par la boîte à outils Gads. Ensuite, 60 SRPFD ont été sélectionnés pour analyser la réponse sismique de la structure du bâtiment. Les résultats montrent que l'effet de contrôle des SRPFD a été amélioré de près de 32,5% après l'optimisation. Les résultats de cette recherche ont permis de mieux comprendre le contrôle d'optimisation semi-actif des modèles de réseau spatial.*

*KEYWORDS: genetic algorithm (GA), Optimal layout, Piezoelectric friction damper (PFD), Semi-active control.*

MOTS-CLÉS: *algorithme génétique (GA), structure optimale, amortisseur de friction piézoélectrique (PFD), contrôle semi-actif.*

DOI:10.3166/ ACSM.42.503-515 

## 1. Introduction

In order to reduce the hazards of building structure especially in earthquakes and solve the comfort problem caused by vibration, Piezoelectric ceramics are used as intelligent materials in the control of building structures. Piezoelectric ceramics (PC), with its low energy consumption, high bearing capacity, wide frequency response range, has both driving and sensing functions. In particular, the PC boasts positive and inverse piezoelectric effects, that is, it can product voltage when subjected to external forces or mechanical pressure (Uchino, 2000; Moulson *et al*., 2003; Jaffe *et al*., 1971). Over the years, the effects have been fully utilized in the piezoelectric friction damper (PFD), a popular tool for the vibration control of intelligent semi-active control dampers (Yamamoto *et al*., 2001; Senousy *et al*., 2009; Liu *et al*., 2009; Zhao and Li. 2010).

Various types of PFDs have been designed by scholars at home and aboard. For example, Ou *et al*. (1999) and Yang *et al*. (2005) proposed a new T-type PFD based on the features of multilayer piezoelectric actuator and Pall friction damper. Qu *et al*. (2000) studied the semi-active control of the wind effect in the steel high-rises installed with PFD. Through numerical analysis and experimental research, Chen *et al*. (2004) verified the effectiveness of a PFD designed for seismic response of building structure control (Chen *et al*., 2004; Ghaffarzadeh *et al*., 2013; Kannan *et al*., 2014; Pardo-Varela *et al*., 2015; Zhao *et al*., 2016; Amjadian *et al*. 2017). All the above studies have paved the way for further research into the development and application of PFD. But different dampers have different characteristics, different dampers have different control effect.

In this paper, a new devices named the self-reset piezoelectric friction damper (SPFD) was designed with the laminated piezoelectric ceramics (PC), and evaluates the damping effect of the SRPFD by the semi-active control strategy and the classical optimal control theory. As its name suggests, the SRPFD is featured by the self-reset function. The PC materials were used to provide driving force to adjust friction under lateral confined compression, the genetic algorithm (GA) was introduced to optimize the number and location of dampers.

## 2. Structure of SRPFD and damping force model

### *2.1. Structure of SRPFD*

As shown in Figures 1 and 2, the SRPFD consists of a piston transmission system, a self-reset system and a piezoelectric friction system. The piston is made up of a dowel bar, a base plate, a top plate and a spherical support.

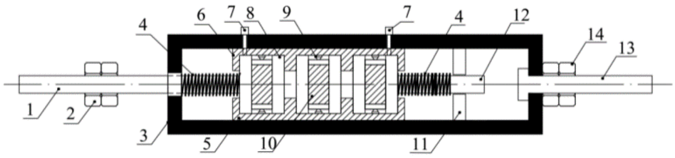


*Figure 1. Schematic diagram of SRPFD ((1) Dowel bar; (2) Limit hexagon nut; (3) Shell; (4) Reset spring; (5) Base plate; (6) Crown sheet; (7) Tightening screw; (8) Drive sleeve; (9) Hemispherical support; (10) Piezoelectric ceramics; (11) Limit baffle; (12) Balance bar; (13) Connecting bar; (14) Fixing screw)*


*Figure 2. Model of SRPFD*

*Figure 3. PC*

Several tightening screws were designed to adjust the interface pre-pressure between the top plate and the inner wall of the shell. The tightening screw on the top plate of the shell can be adjusted as required. The PC (Figure 3), as the driving element, was placed in the sleeves and connected with the circuit system. The upper end of the PC was joined to the top plate, and the lower end to the base plate. Three sleeves were arranged to prevent lateral force and protect the piezoelectric actuator in the piston. When the voltage changes, the driving force will change the friction pressure between the base plate, the top plate and the shell. Two reset springs were provided to ensure the returning of the piston to its original position in the self-reset system.

The SRPFD was installed in the structure to reduce vibration. The dowel bar transfers force and displacement of the structural member, and the piezoelectric friction system supplies controllable friction. Thus, the sliding friction energy of the base plate, the top plate and the shell can be dissipated. In this way, the structure achieves the vibration control, energy consumption, and semi-active control.

### *2.2. Damping force model*

The shape factor of the PFD is expressed as:

$$K = \frac{1}{\frac{1}{m_p E_p A_p} + \frac{H_b}{m_s H_p E_b A_b}} \tag{1}$$

where $K$ is the shape factor of the SRPFD; $E_p$ is the elastic modulus of the SRPFD; $A_p$ is the cross-sectional area of the SRPFD; $E_b$ is the elastic modulus of the PC; $A_b$ is the elastic modulus of the PC; $H_b$ is the effective height of the PC; $m_p$ is the number of the SRPFD; $m_s$ is the number of tightening screws.

The actuator is considered to be fully constrained, for it is much less stiff than the shell. Hence, $E_bA_b$ tends to infinity, and formula (1) can be simplified as $K= E_pA_p$.

Since the piston movement rests in a cycle, there is no total work done by the spring damping force. During vibration, the spring is only responsible for resetting, and consumes no energy. Therefore, the effect of the spring on the damper control force is negligible. Assuming that the friction coefficient of the piston, the top plate and bottom plate is small, then the PFD control force can be expressed as:

$$f(t) = 2\mu\left(N_0 + \frac{N_0+E_pA_pd_{33}U}{d}\right)sgn\left[\dot{X}(t)\right] \tag{2}$$

where $\mu$ is the friction coefficient; $N_0$ is the initial pressure of the PFD; $d_{33}$ is the axial piezoelectric strain constant of the PC; $U$ is the input voltage of piezoelectric actuator; $d$ is the distance between electrodes; $\dot{X}(t)$ is the relative velocity between the shell and the piston of the PFD; Sgn[ ] is a symbolic vector, indicating that the damping force points to the opposite direction of the structure.

The initial pressure of the new PFD is set to $N_0$, and the damping force of the new PFD can be expressed as the friction coefficient between the top plate, the base plate and the damper shell. In this study, the input voltage of the piezoelectric actuator is written as a function of the sliding displacement of the damper. The damping force model of the new PFD can be obtained as:

$$U(t) = U_0\left|\frac{x(t)}{x_{max}}||^n\right| \tag{3}$$

where $U_0$ is the maximum working voltage of a piezoelectric actuator; $x(t)$ is the sliding displacement of damper piston; $x_{max}$ is the maximum design displacement of the damper; $n$ is an exponential indicating the function of input voltage and displacement.

The performance parameters of the PC are as follows: the maximum working voltage $U_0$ is 150V; the elastic modulus EP is 40 GPa; the cross-sectional area $A_p$=10mm×10mm=100mm2; the axial piezoelectric strain constant is $750\times10^{-12}$m/V; the piezoelectric film thickness $d$ is 0.1mm; the friction coefficient of the PFD is 0.25; the maximum design displacement $x_{max}$ is 2cm; the initial pressure $N_0$ is 500N.

## 3. Control strategy

### *3.1. Motion equation*

The space truss model contains three nodes, each of which has 3 degrees of freedom. Thus, the model enjoys a total of 3n degrees of freedom. When the model is under one-dimensional vibration, the control equations of motion are:

$$\begin{cases} M\ddot{X}(t) + C\dot{X}(t) + KX(t) = -M\{I\}\ddot{x}_g + B_s U(t) \\ X(t_0) = X_0 \\ \dot{X}(t_0) = \dot{X}_0 \end{cases} \tag{4}$$

where ***M*** is the structural mass matrix; ***C*** is the damping matrix; ***K*** is the stiffness matrix; n is the number of nodes (all these are 3N order matricies); $\boldsymbol{B}_s$ is the control force position matrix to describe the structure motion in 3n×p coordinates; $X(t)$, $\dot{X}(t)$ and $\ddot{X}(t)$ are the displacement, velocity and acceleration vectors, respectively; {I} is elements are 3n vectors 1; $\ddot{x}$ is the ground acceleration vector; ***U***(*t*) is the p dimension control force column vector. Then, the state vector was introduced as follows:

$$Z(t) = \begin{bmatrix} X[t] \\ \dot{X}(t) \end{bmatrix}_{6n\times 1} \tag{5}$$

Hence, the equation of motion described by the formula (3) can be expressed as the following equation of state:

$$\begin{cases} \dot{Z}(t) = AZ(t) + D\ddot{x}_g + BU(t) \\ Z(t_0) = Z_0 \end{cases} \tag{6}$$

where

$$A = \begin{bmatrix} 0_{3n} & I_{3n} \\ -M^{-1}K & -M^{-1}C \end{bmatrix}_{6n\times 6n}; B = \begin{bmatrix} 0_{3n\times p} \\ -M^{-1}B_S \end{bmatrix}_{6n\times p}; D = \begin{bmatrix} 0_{3n\times 1} \\ -M^{-1}M\{1\} \end{bmatrix}_{6n\times 1}.$$

The $\boldsymbol{I}_{3n} \in \boldsymbol{R}^{3n\times 3n}$ is a unit matrix; **0** is 3n×p zero matrix. For some or all states of the controlled structure system, the m-dimensional output equation is assumed to be:

$$Y(t) = C_0 Z(t) + D_0\ddot{x}_g + B_0 U(t) \tag{7}$$

where $\boldsymbol{C}_0$ is the state output m×2n matrix of the structural system; $\boldsymbol{D}_0$ is the interference m×1 matrix of the structural system; $\boldsymbol{B}_0$ is the control force output m×p matrix of the structural system. The active control algorithm of the structure aims to find the optimal control force vector *U*(*t*) by formulas (6) and (7).

### 3.1. Semi-active control strategy

The optimal control force is designed by the linear–quadratic regulator (LQR) algorithm *u*. The maximum damping force $f_{\max}$ of the PFD equals the maximum active optimal control force $u_{max}$. It is assumed that the PDF control is the same as the active optimal control. Thus, the friction force of the PFD can be approximated to the active optimal control force by adjusting the voltage of the piezoelectric actuator.

The rules of the semi-active control force of each PFD are as follows:

$$f = \begin{cases} f_{max} & ; u\dot{x} < 0, |u| > f_{max} \\ |u|\, sgn(\dot{x}); & u\dot{x} < 0, |u| < f_{max} \\ f_{min} & u\dot{x} \geq 0 \end{cases} \tag{8}$$

## 4. Structure model and optimization algorithm

### *4.1. Structure model*

This section introduces the GA to optimize the number and location of dampers. As shown in Figure 4, a large 24m×24m square pyramid space truss structure was established with the mesh size of 4m×4m. The structure is 24m along the x-axis and 24m along the y-axis. The height of the space truss is 2m, and the bottom of the frame is constrained by the nodes around the bottom grid with three-direction hinge bearings.

There is a total of 85 joint and 288 members, all of which were made of Q235B steel pipes. The other parameters were configured as follows: the upper suspension bar is Φ168×12; the web member is Φ133×8; the bottom chord is Φ159×10; the elastic modulus is 206GPa; the Poisson's ratio is 0.3; the density is $7.85\times10^3$kg/m$^3$. Moreover, the distribution of the mass was assumed to be 200kg/m$^2$ and concentrated on the nodes. The elastic assumption was adopted in the calculation and analysis, and the bar element (link180) was selected in the ANSYS finite-element software.

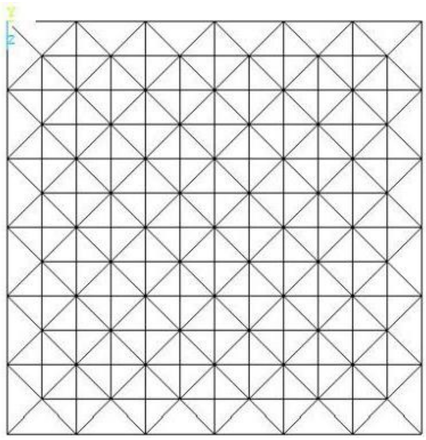

*Figure 4. Finite element model of four square pyramid space truss*

### *4.2. Arrangement of SRPFDs*

In view of the arrangement of SMA compound viscous damping rods, a multi-modal damping control was adopted for the analysis. To optimize the location of damping rod, the performance index was introduced as the following equation of state:

$$J = \sum_{i=1}^{n} \gamma_i \sigma_i^2 \quad (9)$$

where $J$ is the performance index; $\gamma_i$ is the relative importance of the $i$-th controlled mode in the structure; $\sigma_i$ is degree of controlled subject to the $i$-th controlled mode in the structure; n is the number of controlled modes in the structure. Since the control object is mainly the seismic response of the grid structure, the value of $\gamma_i$ can be taken as the corresponding value of $\omega_i$ on the seismic influence coefficient curve. There is a positive correlation among the value of the performance index, the location quality of the damping rod, and the control effect of the structure.

Formula (9) was taken as the objective function for disclosing the effect of the number and position of damping rods on the vibration control of space truss structure. The fitness function can be designed by the basic principle of the GA:

$$\text{Fitness}=\frac{1}{J} \quad (10)$$

According to the formula above, the individual fitness is negatively correlated with the value of the objective function and the quality of damper arrangement.

The GA was employed to optimize the location of the damping rods. The relevant parameters are listed in Table 1. Figure 5 compares the performance indices of different dampers.

*Table 1. Table caption*

| Quantity of SRPFD | Initial population | Max algebra | Crossover probability | Mutation probability |
|---|---|---|---|---|
| 30/60/90/120/150/180/210/240/270 | Can be | 400 | 0.8 | 0.05 |

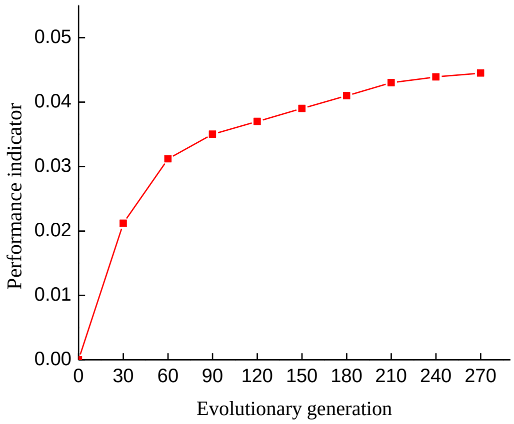


*Figure 5. Comparison of the performance index of different damping rod*

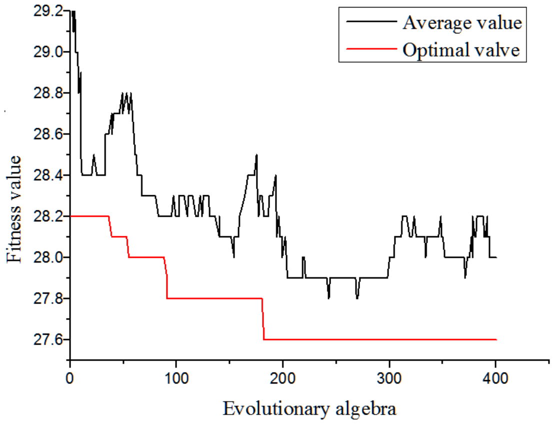


*Figure 6. Convergence process*

As shown in Figure 5, the performance index increased gradually with the increase of the number of damping rods, that is, the improvement of the damping effect. When the number of damping rods reached 60, the performance index tended to be stable. Considering the damping effect and the cost of the SRPFD, the number of dampers was determined to be 60. The convergence to the optimal individual is illustrated in Figure 6, and the optimal arrangement of dampers is presented in Figure 7, where the damping rods are in red and the common bars are in black.

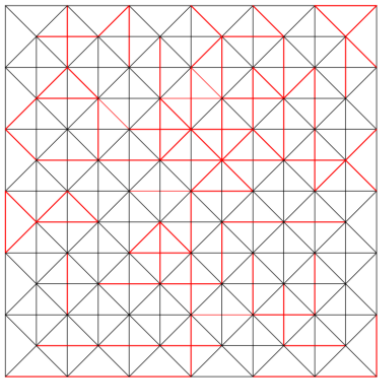

*Figure 7. Arrangement of damping bar (red)*

The GA was optimized by the Gads Matlab toolbox, such that only the minimum value of fitness function can be obtained. Thus, the performance index of the fitness function should be adjusted as follow:

$$\text{Fit}= -J(J - J \times |p - m|) \tag{10}$$

where $J$ is the performance index (the larger its value, the more suitable it is for the next generation); $p$ is the current arrangement of SRPFD; $m$ is the expected arrangement of SRPFD.

In the operation, the control parameters of the GA were configured as follows. The binary coded program was used, with r representing the optimal position of dampers in space truss structure. If there was a damper, r=1; otherwise, r=0.

The initial population size $P_{OP}$ was selected as 20. To find the global optimum and avoid premature convergence, the selection operation was carried out by the ranking selection method. The crossover operation was a two-point crossover at the probability $P_c$ of 0.85. The mutation probability $P_m$ was set to 0.04. The operation of the GA should terminate after reaching to 200th generation. The iteration went on stably for 1,200s, covering 100 generations.

## 5. Semi-active optimization control

### *5.1. Optimization results*

A total of 60 SRPFDs were selected for the seismic response analysis of the structure. In the space truss model, 60 PFDs were separately arranged to replace the damping rods. The layout of damper position was optimized by the GA toolbox of Matlab. Table 2 shows the parameters and position of arrangement.

*Table 2. Optimized parameters and position for SRPFD*

| Type | Quantity of SRPFD | Arranged position of SRPFD / rod |
|---|---|---|
| Optim ized | 60 | 15, 20, 31, 50, 61, 62, 69, 76, 81, 87, 89, 90, 95 100 103 114 116 122 124 130 131 137 141 142 143 157 158 160 162 165 172 175 178 184 203 206 207 213 214 216 218 220 222 223 228 235 238 243 246 247 249 253 257 260 263 264 266 270 281 287 |
| rando m | 60 | 2, 4, 6, 7, 11, 18, 21, 30, 31, 38, 42, 50, 53, 76, 77, 78, 79, 80, 90, 97, 100, 104, 114, 115, 119, 120, 126, 127, 130, 132, 138, 143, 162, 169, 170, 174, 175, 184, 187, 195 , 198, 206, 208, 214, 217, 220, 227, 229, 233, 236, 243, 248, 254, 259, 262, 266, 268, 270, 272, 283 |

### *5.2. Semi-active control analysis and results*

The El Centro seismic wave and the peak acceleration (400gal) of a magnitude 8 earthquake were selected for the analysis. The response and control effect of the no-control, optimal control and random control cases were studied with a loading duration of 20s and loading interval of 0.02s along the x direction of the structure. Through the analysis, node 25, an intermediate node, was selected to demonstrate the displacement response and velocity response of the structure.

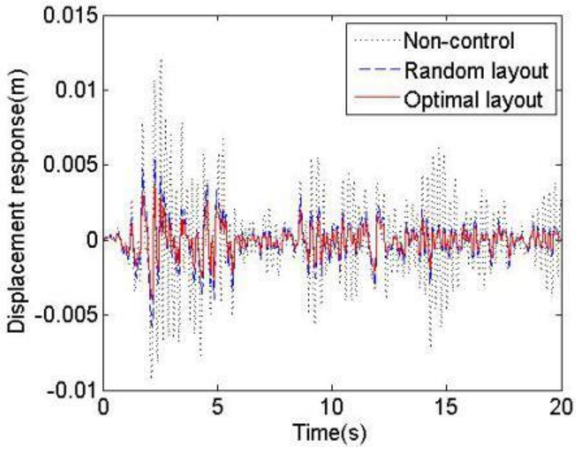


*Figure 8. Displacement-time curve of node 25 with different quantity SRPFDs*

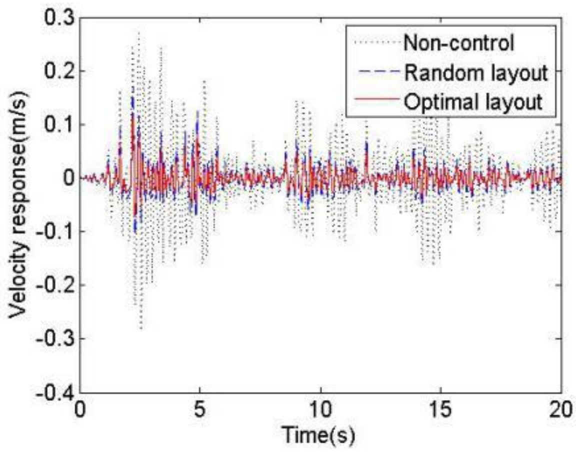


*Figure 9. Velocity -time curve of node 25 with different quantity SRPFDs*

Figures 8 and 9 show the time-displacement and time-velocity curves at different number of SRPFDs of the no-control, optimal control and random control cases. The peak displacement response of the model structure and the corresponding control results are recorded in Table 3.

*Table 3. The control effect of Node 25*

| Quantity of SRPFD | Peak displacement of Node 25 /mm | | | $\alpha$/% | $\beta$/% |
|---|---|---|---|---|---|
| | No control | Optimized | random | | |
| 60 | 12.20 | 4.13 | 6.12 | 66.1 | 32.5 |

where $\alpha = (d_n - d_o)/ d_n \times 100\%$; $\beta = (d_r - d_o)/ d_r \times 100\%$; $\alpha$ is the coefficient of control effect; $\beta$ is the coefficient of optimization effect; $d_n$ is the peak displacement of no-control case; $d_o$ is the peak displacement of the optimal control case; $d_r$ is the peak displacement of the random control case.

With the increase in the number of dampers, the displacement control effect of node 25 steadily improved, but the increment of control effect gradually reduced. Based on the semi-active control strategy of the LQR, the GA-improved structure suffered from a 32.5% lower seismic impact than that of the random control case.

## 6. Conclusions

The design of the SRPFD is so reasonable that the piezoelectric actuator can only be compressed axially. Besides, the SRPFD is compact, easy to install/remove, and applicable to the semi-active seismic control of buildings.

With the increase in the number of dampers, the displacement control effect of node 25 steadily improved, but the increment of control effect gradually reduced. This means the selected damper vibration control strategy is both effective and cost-efficient.

The damper arrangement was optimized by the semi-active control strategy based on the LQR algorithm. The control effect of the PFD was improved by nearly 32.5% after optimization.

*Acknowledgment*

*The authors gratefully acknowledge the support of the Scientific Research Program Funded by Shaanxi Provincial Education Department (Program No.17JK0072).*

## References

Amjadian M., Agrawal A. K. (2017). A passive electromagnetic eddy current friction damper (PEMECFD). Theoretical and analytical modeling. *Structural Control and Health Monitoring*, Vol. 24, No. 10, pp. 1-23. https://doi.org/10.1002/stc.1978

Chen C. Q., Chen G. D. (2004). Shake table tests of a quarter-scale three-story building model with piezoelectric friction dampers. *Structural Control and Health Monitoring*, Vol. 11, No. 4, pp. 239-257. https://doi.org/10.1002/stc.41

Chen G. D., Garrett G. T., Chen C. Q., Cheng F. (2004). Piezoelectric friction dampers for earthquake mitigation of buildings design fabrication and characterization. *Structural Engineering and Mechanics*, Vol. 17, No. 3-4, pp. 539-556. https://doi.org/10.12989/sem.2004.17.3_4.539

Ghaffarzadeh H., Dehrod E. A., Talebian N. (2013). Semi-active fuzzy control for seismic response reduction of building frames using variable orifice dampers subjected to near-fault earthquakes. *Journal of Vibration and Control*, Vol. 19, No. 13, pp. 1980-1999. https://doi.org/10.1177/1077546312449179

Jaffe B., Cook W. R., Jaffe H. (1971). *Piezoelectric ceramics*. Academic Press, London.

Kannan S., Uras H. M., Aktan H. M. (1995). Active control of building seismic response by energy dissipation. *Earthquake Engineering & Structural Dynamics*, Vol. 24, pp. 747-759. https://doi.org/10.1002/eqe.4290240510

Laflamme S., Taylor D., Maane M. A., Connor J. J. (2012). Modified friction device for control of large-scale systems. *Structural Control and Health Monitoring*, Vol. 19, No. 4, pp. 548-64. https://doi.org/10.1002/stc.454

Liu W. F., Ren X. B. (2009), Large piezoelectric effect in Pb-free ceramics. *Phys RevLett*, Vol. 103, No. 25. pp. 1-4. https://doi.org/10.1103/PhysRevLett.103.257602

Moulson A. J., Herbert J. M. (2003). *Electroceramics: Materials, Properties, Applications*. Wiley, Chichester.

Ou J. P., Guan X. C. (1999). Research and development of civil engineering intelligent structure system. *Earthquake Engineering and Engineering Vibration*, Vol. 12, No. 2, pp. 21-28. https://doi.org/10.13197/j.eeev.1999.02.004

Pardo-Varela J., de la Llera J. C. (2015). A Semi-active piezoelectric friction damper. *Earthquake Engineering & Structural Dynamics*, Vol. 44, No. 3. pp. 333-354. https://doi.org/10.1002/eqe.2469

Qu W. L., Chen Z. H., Xu Y. L. (2000). Wind-induced vibration control of high-rise steel-truss tower using piezoelectric smart friction dampers. *Journal of Earthquake Engineering and Engineering Vibration*, Vol. 20, No. 1, pp. 94-99. https://doi.org/10.13197/j.eeev.2000.01.014

Senousy M. S., Rajapakse R. K. N. D., Mumford D., Gadala M. S. (2009). Self-heat generation in piezoelectric stack actuators used in fuel injectors. *Smart Mater Struct*, Vol.,18, No. 4. https://doi.org/10.1088/0964-1726/18/4/045008

Uchino K. (2000). *Ferroelectric devices*. Marcel Dekker, New York.

Yamamoto M., Aizawa S., Higashino M., Toyama K. (2001). Practical application of active mass dampers with hydraulic actuator. *Earthquake Engineering and Structural Dynamics*, Vol. 30, No. 11, pp. 1697-1717. https://doi.org/10.1002/eqe.88

Yang Y., Ou J. P. (2005), Numerical analysis of piezoelectric variable friction damper vibration attenuation structure. *Journal of Vibration and Shock*, Vol. 24, No. 6, pp. 1-4. https://doi.org/10.13465/j.cnki.jvs.2005.06.001

Zhao D. H., Li H. N. (2010). Shaking table tests and analyses of semi-active fuzzy control for structural seismic reduction with a piezoelectric variable friction damper. *Smart Materials and Structures*, Vol. 19, No. 10, pp. 105031. https://doi.org/10.1088/0964-1726/19/10/105031

Zhao D. H., Li Y. X., Li H. N., Qian H. (2016). Research on semi-active isolation structure based on multi-stage fuzzy control. *Journal of Vibration and Shock*, Vol. 35, No. 13, pp. 78-84. https://doi.org/10.13465/j.cnki.jvs.2016.13.013